NeuroImage 59 (2012) 2035–2044

Contents lists available at SciVerse ScienceDirect

NeuroImage

journal homepage: www.elsevier.com/locate/ynimg

High resolution MR anatomy of the subthalamic nucleus: Imaging at 9.4 T with histological validation

L.A. Massey [a,b,*], M.A. Miranda [c], L. Zrinzo [h], O. Al-Helli [a,e], H.G. Parkes [e], J.S. Thornton [e,f], P.-W. So [g], M.J. White [e,f], L. Mancini [e,f], C. Strand [b], J.L. Holton [b], M.I. Hariz [h], A.J. Lees [a,b,d], T. Revesz [b], T.A. Yousry [e,f]

[a] Sara Koe PSP Research Centre, UCL Institute of Neurology, London, UK
[b] Queen Square Brain Bank for Neurological Disorders, UCL Institute of Neurology, London, UK
[c] Division of Radiology, Department of Medicine, School of Medicine, University of Panama, Panama City, Panama
[d] Reta Lila Weston Institute of Neurological Studies, UCL Institute of Neurology, London, UK
[e] Department of Brain Repair and Rehabilitation, UCL Institute of Neurology, London, UK
[f] Lysholm Department of Neuroradiology, National Hospital for Neurology and Neurosurgery, Queen Square, London, UK
[g] King's College London, Preclinical Imaging Unit, Department of Neuroimaging, Institute of Psychiatry, London, UK
[h] Unit of Functional Neurosurgery, UCL Institute of Neurology, Queen Square, London, UK

ARTICLE INFO

Article history:
Received 30 June 2011
Revised 21 September 2011
Accepted 5 October 2011
Available online 21 October 2011

Keywords:
High Field MRI
Subthalamic nucleus
Pathological validation

ABSTRACT

Using conventional MRI the subthalamic nucleus (STN) is not clearly defined. Our objective was to define the anatomy of the STN using 9.4 T MRI of post mortem tissue with histological validation. Spin-echo (SE) and 3D gradient-echo (GE) images were obtained at 9.4 T in 8 post mortem tissue blocks and compared directly with corresponding histological slides prepared with Luxol Fast Blue/Cresyl Violet (LFB/CV) in 4 cases and Perl stain in 3. The variability of the STN anatomy was studied using internal reference points. The anatomy of the STN and surrounding structures was demonstrated in all three anatomical planes using 9.4 T MR images in concordance with LFB/CV stained histological sections. Signal hypointensity was seen in 6/8 cases in the anterior and medial STN that corresponded with regions of more intense Perl staining. There was significant variability in the volume, shape and location of the borders of the STN. Using 9.4 T MRI, the internal signal characteristics and borders of the STN are clearly defined and significant anatomical variability is apparent. Direct visualisation of the STN is possible using high field MRI and this is particularly relevant, given its anatomical variability, for planning deep brain stimulation.

Introduction

The subthalamic nucleus (STN) was first described by Jules Bernard Luys (1828–1897) in 1865(Parent, 2002). In the early 20th century Purdon Martin identified vascular lesions in the subthalamic region in cases of hemiballism (Purdon Martin, 1927). More recent studies demonstrate improvement in Parkinsonian symptoms in the 1-methyl-4-phenyl-1,2,3,6-tetrahydropyridine (MPTP) monkey model of Parkinsonism is found after placement of lesions (Aziz et al., 1991; Bergman et al., 1990) or high-frequency stimulation of the STN (Benazzouz et al., 1993). As a consequence the STN has become the target of choice for deep brain stimulation in advanced Parkinson's disease (PD) (Limousin et al., 1995, 1998).

The oblique orientation and small size of this structure contribute to the difficulties in its identification using conventional MRI. In planning placement of deep brain electrodes, standard brain atlases are commonly used to derive the coordinates of the STN in relation to the patient's ventricular landmarks obtained by ventriculography (Benabid et al., 2000) or T1-weighted MRI (Starr, 2002), Clinical and electrophysiological surrogates are used to confirm electrode placement (Gross et al., 2006). However, the anatomical accuracy of this

Abbreviations: A, Anterior; AC, Anterior commissure; AL, Ansa lenticularis; CC, Crus cerebri; CM, Centromedian nucleus of the thalamus; DTT, Dorsal tegmental tract; F, Fornix; FMT, Fornix-mammillothalamic tract; FR, Fasciculus retroflexus; GE, Gradient echo; GP, Globus pallidus; GPi, Globus pallidus internal segment; H, H field of Forel; H1, H1 field of Forel; H2, H2 field of Forel; Hab, Habenular nucleus; HabC, Commissure of the habenular nucleus; Hyp, Hypothalamus; I, Inferior; IC, Internal capsule; III, third ventricle; IML, Internal medullary lamina; LF, Lenticular fasciculus; LFB/CV, Luxol fast blue/cresyl violet; LGB, Lateral geniculate body; MB, Mammillary body; MGB, Medial geniculate body; ML, Medial lemniscus; MTT, Mammillothalamic tract; OT, Optic tract; GP, Globus pallidus; P, Posterior; PC, Posterior commissure; PT, Pyramidal tract; Pulv, Pulvinar; Q, Pallidoreticular bundle Q of Sano; QSBB, Queen square brain bank for neurological disorders; RCTF, Rubro-cerebello-thalamic fascicles; RN, Red nucleus; S, Superior; SE, Spin Echo; SF, Subthalamic fasciculus; SN, Substantia nigra; STN, Subthalamic nucleus; STT, Spinothalamic tract; SupC, Superior colliculus; T, Tesla; TE, Echo time; TF, Thalamic fasciculus; Th, Thalamus; TR, Repetition time; ZI, Zona incerta.

* Corresponding author at: Sara Koe PSP Research Centre, UCL Institute of Neurology, 1 Wakefield Street, London, WC1N 1PJ, UK. Fax: +44 20 7278 4993.
E-mail addresses: l.massey@ion.ucl.ac.uk (L.A. Massey), mm.miramar@gmail.com (M.A. Miranda), l.zrinzo@ion.ucl.ac.uk (L. Zrinzo), o.al-helli@ion.ucl.ac.uk (O. Al-Helli), hgparkes@yahoo.co.uk (H.G. Parkes), john.thornton@uclh.nhs.uk (J.S. Thornton), po-wah.so@kcl.ac.uk (P.-W. So), mark.white@ucl.ac.uk (M.J. White), laura.mancini@uclh.nhs.uk (L. Mancini), c.strand@ion.ucl.ac.uk (C. Strand), J.Holton@ion.ucl.ac.uk (J.L. Holton), m.hariz@ion.ucl.ac.uk (M.I. Hariz), a.lees@ion.ucl.ac.uk (A.J. Lees), t.revesz@ion.ucl.ac.uk (T. Revesz), t.yousry@ion.ucl.ac.uk (T.A. Yousry).

1053-8119/$ – see front matter © 2011 Elsevier Inc. All rights reserved.
doi:10.1016/j.neuroimage.2011.10.016

approach has been challenged by pathological reports of inaccuracies in electrode placement (Counelis et al., 2003; Hariz et al., 2004; McClelland et al., 2007) and by demonstration of the inter-individual variability in the shape, size and position of the STN (Ashkan et al., 2007; den Dunnen and Staal, 2005). Direct visualisation of the STN is reported using reproducible MRI methods (Foltynie et al., 2011; Hariz et al., 2003, 2004; Zonenshayn et al., 2000). However, a further study has suggested that the STN is only partially visualised on conventional MRI at 1.5 T (Dormont et al., 2004).

The accuracy of MR in visualising structures such as the STN is best assessed by comparing its characteristics on MR directly with those revealed histologically. Thus far there has been no direct comparison between the STN visualisation on MRI and its histological characteristics in the same specimen. We aimed to validate directly the anatomical definition of the STN using high field MRI with histological examination of the same tissue and to determine the anatomical variability of this nucleus.

Materials and methods

Preparation of post mortem tissue

Post mortem brain tissue was obtained from the Queen Square Brain Bank for Neurological Disorders (QSBB), UCL Institute of Neurology, where tissue is donated according to ethically approved protocols and is stored under a licence from the Human Tissue Authority. Eight specimens were used in this study [Table 1]. Formalin-fixed tissue was dissected to produce a tissue block that included the subthalamic nucleus. The MR axis was aligned perpendicular to the axis of the brainstem and, after imaging, the specimen was divided along this midline sagittal axis before embedding in paraffin.

MRI protocol

Samples were imaged at room temperature in *perfluoropolyether* (Fomblin, Solvay Selexis) at 9.4 T (Varian NMRS MRI) with a 40 mm quadrature volume RF coil.

1. Parameters for high-resolution spin-echo (SE) images were: TE 15–22 ms, TR 2000–2200 ms, scan averages 24–32, interleaved slices, slice thickness 0.5–1 mm, slice gap 0.5–1 mm, matrix 512×512, field of view (FOV) 45×45 mm (in-plane resolution 88 μm) and imaging time up to 10 hours.
2. Superior in-plane resolution was obtained in one case: 1024×1024 matrix (in plane resolution 44 μm), 132 averages; other parameters as above, imaging time 72 hours.
3. Three dimensional gradient echo (ge3d) sequences had the following parameters: TR 12 ms, TE 3.2 ms, flip angle 10°, FOV 45 mm×45 mm×90 mm, Matrix 256×256×512, 14 averages, acquisition time 3 hours 4 minutes.

These parameters were chosen on the basis of pilot acquisitions to yield optimal image contrast for the structures of interest; due to the reduced T2 relaxation times in fixed tissue at 9.4 T (unpublished data) the SE sequence parameters produced predominantly T2-weighted image contrast. Images were viewed and processed in ImageJ (version 1.43 h, US National Institutes of Health, Bethesda, Maryland) (Rasbrand, 2009).

Histological protocol

After imaging tissue blocks were cut and embedded in paraffin wax and serially sectioned at 20 mm. Every 20th section was stained with the Luxol Fast Blue and Cresyl Violet (LFB/CV) method in 4 cases, and in 3 of these further sections were stained with Perl's stain for iron. Macroscopic images were obtained at 20–40× magnification using Image Pro Plus (Mediacybernetics, Bethseda, MD www.mediacy.com).

Image segmentation, orientation, dimensions and volume calculations

MR images were segmented manually in ITK-SNAP (version 1.8.0) (Yushkevich et al., 2006) with reference to neuroanatomical atlases (Carpenter and Sutin, 1983; Nieuwenhuys et al., 1988, 2008; Schaltenbrand and Wahren, 1977). After manual segmentation the STN volume was calculated using the volume and statistics function. Segmentation-mask measurements of the STN width (maximum distance in the axial plane from medial to lateral tip) and depth (maximum distance in the axial plane between the anterior and posterior borders perpendicular to the width measurement) in the axial plane were obtained with ImageJ; the height was calculated with reference to the number of 1–1.5 mm axial slices in which the STN appeared. The higher-contrast SE images were used for calculation of volume and measurements. Ge3d images were used to demonstrate the relationship of structures in three dimensions due the their intrinsic higher resolution in all 3 orthogonal planes.

Position relative to internal markers

The position of the STN was determined in relationship to three arbitrary lines in the axial plane [Fig. 1]:

1. The midline
2. A line connecting the anterior border of the fornix with the posterior border of the mamillothalamic tract (*the FMT line*)
3. A line parallel to the axis of the myelinated fibres separating the substantia nigra (SN) and red nucleus (RN) (*the RN line*) through the maximum diameter of the red nucleus

The position of the STN itself was represented by a line connecting the posterolateral and the anteromedial tip of the STN (the STN line). The FMT line and STN line were used as reference at all levels. The RN line however; was not used at levels above the RN, the transverse

Table 1
Characteristics of cases studied.

No	Gender	Side fixed	Age at death	DOF (days)	Pathological diagnosis	Cause of death
1	F	Both	94	4149	Tissue not examined pathologically	"Old age"
2	M	Right	94	51	1. Small vessel disease (severe 2. Braak and Braak stage IV	Broncho-pneuomonia
3	M	Right	38	56	1. No diagnosis made	Metastatic disease
4	M	Left	78	78	1. Cerebral amyloid angiopathy (moderate)	Metastatic carcinoma of the lung
5	M	Right	79	1029	1. No diagnosis made	1. bilateral broncho-pneumonia 2. possible metastatic disease
6	F	Left	82	366	1. Pathological ageing 2. moderate cerebral amyloid angiopathy 3. mild small vessel disease	
7	F	Right	82	302	1. Control 2. Pathological Ageing 3. Parietal Infarct	1. Broncho-pneumonia
8	F	Right	72	67	1. Amyotrophic lateral sclerosis	1. Metastatic disease

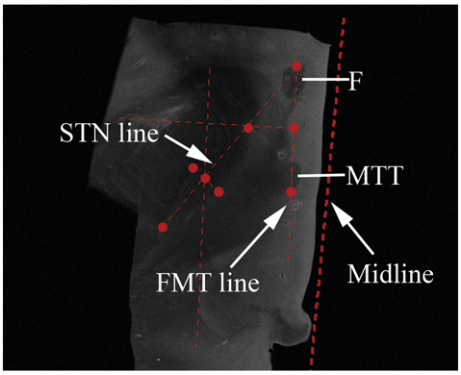

Fig. 1. Assessing the anatomical variability of the STN at 9.4 T. SE axial image through a superior level of the STN with the MTT and F clearly identifiable. Reference points are the midline, and the midpoint between the F and MTT. Measured points are marked as red dots and included the medial and lateral tips, the anterior and posterior borders of the STN. See text.

myelinated fibres have a more circular shape at this level and are thus less amenable to being used as a reliable marker of axis. SPSS 16.0 for Mac (Microsoft, Redmond, WA) was used for statistical analysis.

Results

Shape and signal characteristics of the STN on SE images

Excellent contrast between white and grey matter allowed clear definition of the STN boundaries on SE images in all cases. In the axial plane, the STN was almond shaped and lay at an oblique angle to the anteroposterior (AP) axis of the brainstem [Fig. 2]. In 5/8 cases studied (6/9 nuclei) the STN was of intermediate signal intensity, similar to that of the internal capsule and between that of grey matter structures such as the pulvinar and hypothalamus which appeared hyperintense, and that of the pallidum, ansa lenticularis (AL), RN and SN which were hypointense [Fig. 2]. In 2 cases (long duration fixation) the signal arising from the STN was higher and in one the STN was relatively hypointense and comparable to other iron-laden nuclei. The anteromedial portion of the STN was relatively hypointense in 6/8 cases compared to the posterolateral portion [Figs. 2A–D short white arrow].

Position of the STN

Axial SE images were available in all cases; additional coronal and sagittal SE images were available in one [Figs. 3 and 4]. The STN lay obliquely in all three planes. In the axial plane, the STN was approximately 40 degrees oblique to the midline: at the more superior level studied the mean angle was 42.8 degrees (SD 7.3) and at the inferior level studied 38.1 degrees (SD 3.8) [Table 4b]; in the sagittal plane 35 degrees oblique to the vertical axis [Fig. 3] and in the coronal plane 50 degrees oblique to the midline [Fig. 4].

Borders of the STN

The anterior border of the STN was formed by the internal capsule superiorly [Figs. 2A–D, 3B, 4C] and the substantia nigra inferiorly [Figs. 2E, 3C–G, 4A–E arrowed]. The STN was outlined by a rim of hypointensity, particularly at more inferior levels, in all cases [Figs. 2D–F]. The SN enveloped the anterior and inferior aspect of the STN at the level of the optic tract [Figs. 3A–G], with the zona incerta (ZI) running along the posterior and superior surface [Figs. 3C–E] and the lenticular fasciculus (LF, H2 field of Forel) at the most superior aspect of the STN [Figs. 3D–F]. In more medial sagittal slices, the ansa lenticularis (AL) was seen sweeping around the medial internal capsule [Figs. 3F and G] forming part of the medial and anterior border of the STN. The AL was also seen joining H2 to form the H Field of Forel [Figs. 3F–G] and the thalamic fasciculus (H1) [Figs. 3B–F]. The anterior and medial border was clearly defined,

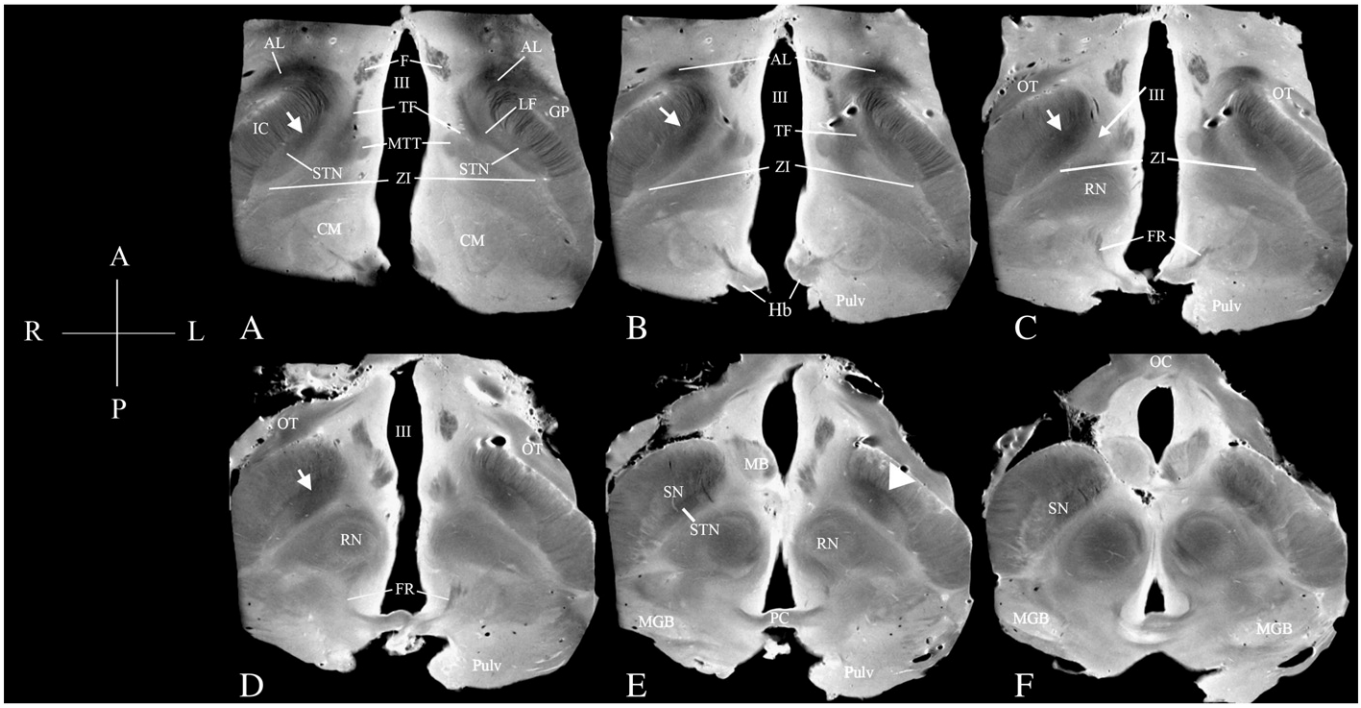

Fig. 2. Axial Plane. The anatomy of the STN on SE MRI at 9.4 T showing both halves of the midbrain in serial axial sections from superior to inferior levels [A-F]. Long white arrow: anteromedial border of the STN defined by the confluence of the ZI and posterior border of the hypothalamus. Short white arrow: medial hypointensity of the STN (seen in 6/9 subthalamic nuclei studied). Arrow head in 2E identifying the hypointense band forming the anterior border of the STN and enabling discrimination from the SN at more inferior levels—see 2E on the right side the most inferior portion of the STN can distinguished medial to the SN. Acquired with an in-plane resolution of 88 μm. Orientation: A—anterior, P—posterior, M—medial, L—lateral.

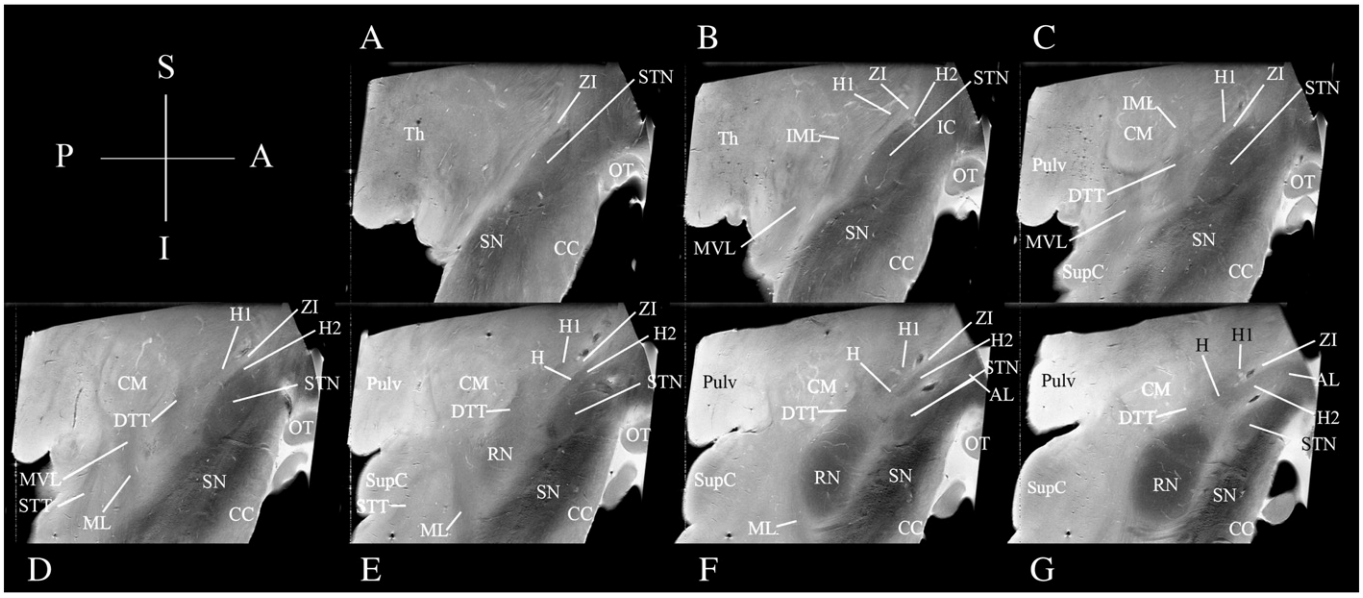

Fig. 3. Sagittal plane. The STN in serial 1 mm sagittal sections from lateral to medial [A–G]. Acquired with an in-plane resolution of 88 μm. Orientation: S—superior, I—inferior, P—posterior, A—anterior.

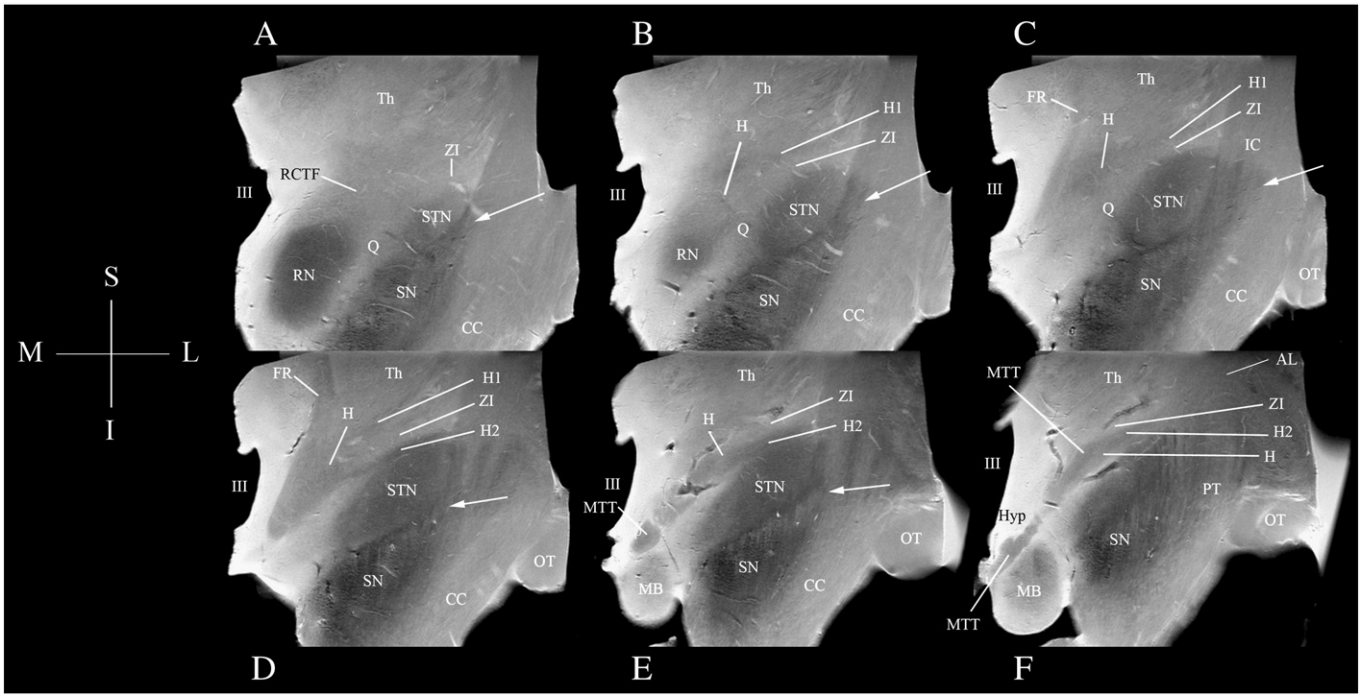

Fig. 4. Coronal plane: The STN in serial 1 mm coronal sections in a control case from posterior to anterior [A–F]. The SN can be seen enveloping the inferolateral border of the STN (white arrow). Acquired with an in-plane resolution of 88 μm. Orientation: S—superior, I—inferior, M—medial, L—lateral.

bounded by the ZI, and the posterior aspect of the hypothalamus. [Fig. 2C long arrow] (Hamani et al., 2004). The LF also formed the most medial 1/3 of the anterior border of the STN at the most superior level.

The *superior border* of the STN was formed by the LF, seen as a region of hypointensity in all cases in axial sections but best appreciated in the sagittal and coronal planes [Figs. 3D–F, 4D–E]. The LF was seen as a slightly lower intensity structure in MR slices above the STN in the axial, coronal and sagittal planes.

The *posterior border* was formed by a hyperintense band that corresponds to the grey matter of the zona incerta above the level of the RN [Figs. 2A and B]. At lower levels the hyperintense signal arose from tissue between the STN and more caudally the SN and the RN: this is the site of myelinated fibres orientated in the axial plane in a posterolateral–anteromedial axis (Adachi et al., 1999) of the nigrostriatal tract (Adachi et al., 1999; Moore et al., 1971) or the pallidoreticular bundle (bundle Q) (Schaltenbrand and Wahren, 1977).

The *inferior border* of the STN is formed by the SN, which is wrapped around the most inferolateral aspect [Figs. 3A–F, 4A–E white arrow]. It is more difficult to accurately define this boundary in the axial plane [Fig. 2E where the most inferior part of the right STN is seen and Fig. 2F where the most inferior part of the left STN is seen]. The STN returns a slightly higher signal than the SN in 4/8 cases. More importantly, a

Table 2
Dimensions and volume of the STN.

Case number	Max width	Max depth	Max height	Volume (mm^3)
1 (R)	12.0	3.3	6	120
1 (L)	11.4	3.2	6	103
2[a]	12.6	3.3	4.5	83
3	15.5	3.5	7.5	113
4	12.6	3.2	6	100
5	11.5	3.3	7.5	126
6	11	2.9	6	103
7	11.2	2.9	7	95
8	10	2.9	7	87

Mean values (range)*: Max width: 12.0 (10–15.5) mm; Max Depth: 3.2 (2.9–3.5) mm; Max Height: 6.6 (6–7.5) mm; Volume: 106 (87–126) mm^3.
* Mean height and volume calculation excludes case 2 where the imaging data did not cover the entire STN.
[a] Incomplete STN measurement as MRI did not cover entire STN hence for these cases the volume and height are underestimates; (R) right; (L) left.

Table 3
Definition of axes used in studying the STN variability.

Line/axis	Definition
FMT Line	Drawn between the Fornix and Mammillothalamic tract (FMT)
STN line	Drawn across the medial and lateral tips of the STN in the axial plane
Midline	Placed in the midline
RN line	Parallel to the high signal line running between the STN and RN at inferior levels

relatively hypointense signal band was found in all cases enabling separation of STN from SN [Figs. 2C–E, arrow head 2E].

In the cases where higher resolution images acquired with an in plane resolution of 44 μm) were available this also enabled accurate identification of fibres of the subthalamic fasciculus as they pass through the internal capsule [Fig. 5].

Comparison of MR images with LFB/CV stain and Perl stain

MR images with corresponding LFB/CV stained sections were available in 4 cases. Comparison of the SE MR images with the histological sections confirmed a good anatomical correspondence [Fig. 6 and legend].

Perl's stain for iron was performed in 3 cases. At superior levels the most intense staining was seen in the globus pallidus and the AL as it courses around the internal capsule and comes to lie adjacent to the anteromedial tip of the STN [Figs. 7A–C]. The SN was seen at lower levels with intense Perl-positive staining particularly in the most anterior and medial portion [Figs. 7D–F]. The STN itself stained less intensely and the more lateral and posterior portions were least heavily stained in 2/3 cases, particularly in the more inferior sections [Figs. 7B–E]. By comparison the most hypointense signal, correlating to the distribution of most intense Perl staining, was seen in the superior, anterior and medial STN [Fig. 2]. In one case, Perl stain was uniform in the STN and corresponded to uniform hypointensity on high field MR images.

Demonstration of three dimensional relationships of the STN to surrounding structures

We have reconstructed the anatomy of the STN and surrounding structures by manually segmenting the ge3d images. This allowed us to display the relationship of the STN to surrounding structures in three dimensions (Fig. 8).

Measurements of the STN and its landmarks

The volume of the STN was 106 mm^3 on average (range 87–126 mm^3), the maximum width 12 mm, the maximum depth 3.2 mm and the height 6.6 mm [Table 2]. The STN lies at a mean angle of approximately 40 degrees to the midline [Table 4a and b; Fig. 1]. The medial tip is 6 mm, the lateral tip 13.5 mm, the midpoint 10 mm, the posterior boundary 9 mm and the anterior boundary 11 mm to the midline. The posterior boundary lies 4.3 mm (range 3.3–5.2) and the anterior boundary 7.5 mm (range 6.1–8.2) from the centre of the RN [Table 5]. The angle of the FMT line varies as the axial position becomes more inferior as it rotates to increase the angle between itself and the STN and midline. The midpoint of the FMT lies 3.3–3.5 mm lateral to the midline. The medial tip of the STN lies approximately 3 mm lateral to the FMT and within 1 mm of it in the AP axis. The lateral tip and midpoint measurements are more discrepant between the superior and inferior levels based on the FMT line as one might expect given the difference in angle of the FMT with axial position [Table 4a and b]. The position of the STN relative to a midpoint between the Fornix and MTT at superior and inferior levels can be seen in 7/8 cases [Fig. 9]. These scatter plots demonstrate visually the anatomical variability. No significant association was found between the position of the STN and age at death. However, with duration of fixation there was a trend towards an increase in distance for the lateral, anterior and posterior borders and a statistically significant increase in distance of the midpoint of the STN from the midline (Pearson correlation coefficient −0.769, $p = 0.043$ for the STN midpoint). However, this relationship is no longer significant when the outlier with very long fixation time is excluded from the analysis.

Discussion

We have described the anatomy of the STN, its internal structure and anatomic variability seen using high field MRI, with histological validation. On 9.4 T MRI, a variable signal was distinguished within

Table 4
Measurements: angles (SD) in degrees, otherwise linear measurements mean (SD) in mm. *x* is distance medial-lateral; *y* is distance anterior-posterior.

a. Measurements relative to the midpoint between the mamillothalamic tract and the Fornix

	FMT-STN Angle	Medial tip		Lateral tip		Mid point		Dorsal mid point		Ventral mid point	
		x	*y*	*x*	*y*	*x*	*y*	*x*	*y*	*x*	*y*
Sup	42.3 (9.7)	2.9 (1.6)	0.2 (0.6)	10.3 (1.2)	8.6 (1.9)	6.5 (1.2)	4.3 (1.3)	5.3 (0.8)	5.1 (1.2)	7.5 (1.4)	3.6 (1.3)
Inf	57.6 (10.4)	3.2 (1.1)	0.2 (0.7)	12.6 (1.3)	6.6 (2.2)	7.9 (1.3)	3.6 (1.2)	7.1 (0.9)	4.4 (1.2)	8.4 (0.9)	1.9 (1.3)

b. Measurements relative to the midline.

	STN-midline Angle	Medial tip	Lateral tip	Mid point	Dorsal mid point	Ventral mid point
		x	*x*	*x*	*x*	*x*
Sup	42.8 (7.3)	5.8 (1.9)	13.5 (2.0)	9.9 (1.8)	8.9 (1.6)	10.7 (2.0)
Inf	38.1 (3.8)	5.7 (1.3)	13.4 (1.4)	9.7 (1.0)	8.9 (1.2)	11.2 (1.1)

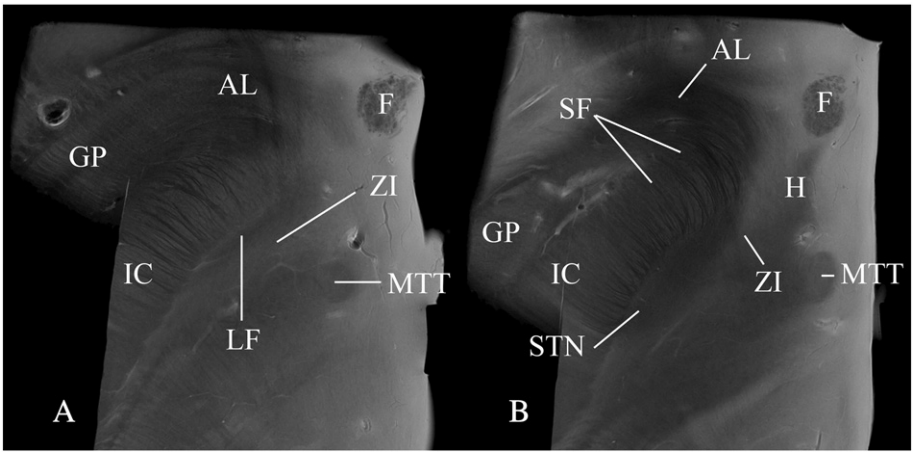

Fig. 5. The STN in the axial plane using SE MRI with image resolution acquired at 44 μm in plane. Panel A just above the level of the STN, Panel B at a superior level of the STN above the RN. The resolution of these images allows clear identification the fibres of the subthalamic fasciculus radiating through the internal capsule.

the STN in 75%, reflecting differences in iron deposition as confirmed by Perl's stain. This anatomical variability confirms the importance of direct STN visualisation when targeting it for stereotactic surgical procedures.

High field MRI of post mortem tissue has been used to define the anatomy of structures difficult to visualise on clinical MRI (Lane et al., 2005; Silver et al., 2002), including the STN (Rijkers et al., 2007). The main advantages of MR microscopy are increased signal to noise ratio (SNR), minimisation of movement artefacts and the ability to image in orthogonal planes with multiple averages. This enables a significant increase in spatial resolution and reduced partial volume effects. We obtained in-plane resolution comparable to macroscopic post-mortem examination - with clear demarcation of the boundaries of the STN and visualisation of small structures such as the subthalamic fasciculus, the lenticular fasciculus and the zona incerta.

The borders of the STN were clearly visualised in all specimens allowing straightforward differentiation from the SN [Figs. 2–4 and 6]. At 1.5 T, the STN returns an apparently homogeneously distributed hypointense signal on T2-weighted MRI (Bejjani et al., 2000; Coenen et al., 2008; Hariz et al., 2003). This hypointense area may only represent one component of the STN; another smaller component may not be visible on MRI or with Perl's stain on histology (Dormont et al., 2004). In our study at 9.4 T, we identified areas of signal variability within the STN in 75% of cases: a relatively hypointense area was located anteromedially and a relatively hyperintense area was located posterolaterally [Fig. 2]. The anatomic location of the latter suggests that it corresponds to the area not consistently visualised at 1.5 T. Perl's stain confirmed the difference in iron deposition suggesting that the difference in T2 signal is related to a difference in tissue iron content. Others have attributed the hypointense signal in the STN to iron (Rutledge et al., 1987), although others have suggested that the high neuronal density of the STN may contribute (Hamani et al., 2005). The signal heterogeneity we observed may be related to the functional subdivision of the STN into three separate territories—the limbic anteromedial part, the associative mid part and the sensorimotor posterolateral part. These functional subdivisions are based on extrapolation from animal work (Karachi et al., 2005; Parent and Hazrati, 1995; Yelnik et al., 2007) but have not, to our knowledge, been specifically shown in humans. It may be this posterolateral or "sensorimotor" portion that is difficult to visualise on lower field conventional MRI. The homogeneous signal in 25% (2/8) of our cases, with histological validation, highlights the degree of variability that can be encountered. It is however important to note that it is not clear whether the STN as visualised clinically at 1.5 T represents a component of the STN or the complete nucleus and this will have a bearing on targeting strategies in functional neurosurgery. However, we would also argue that direct visualisation of a portion of the surgical target is superior to estimating its location based on indirect landmarks.

We have previously studied anatomical accuracy in context of stereotactic targeting of the pedunculopontine nucleus (PPN) for deep brain stimulation (Zrinzo et al., 2011). We were able to validate a method of targeting the PPN by comparing its position as seen on both conventional 1.5 T MRI and high field 9.4 T postmortem MRI, with macroscopic histological images in the same tissue. A similar study comparing conventional and high resolution images with histological material to validate methods for targeting the STN has not yet been undertaken.

In our study, the STN mean volume of 106 mm^3 (range 83–126) is comparable to previous measurements of around 127 mm^3 post mortem in controls (the quoted measurement of 254 mm^3 is for both sides together) (Hardman et al., 1997), 120 mm^3 (assuming that both left and right STN volumes were used in this paper also)(Hardman et al., 2002) and 158 mm^3 (Yelnik, 2002). In a further study the reported STN volume was 174.5 mm^3 but these individuals were younger at the time of death and duration of fixation at the time of measurement shorter (Levesque and Parent, 2005). After formalin fixation and processing into paraffin wax there is marked potentially non-uniform tissue shrinkage (Quester and Schroder, 1997). This has implications when comparing ante mortem with post mortem measurements of volume and linear dimensions which may be significantly affected by the fixation process.

Significant anatomical variability of the STN was found on our histologically-validated high resolution MRI in relation to the midline and other internal structures. At the more inferior level studied, the position of the lateral tip was most variable—this level includes the RN and is close to the target slice used on conventional 1.5 T imaging used for surgical STN planning (Bejjani et al., 2000). This is the region of the STN not so clearly seen on conventional MRI and likely to be a sensorimotor portion of the nucleus. Even small variations in position of the STN in a region where the maximal depth of the STN in the axial plane is only 3.2 mm are likely to be significant. On conventional MRI the medial STN is 8.6 ± 4.3 mm lateral to the midline and the lateral STN 13 ± 6 mm (Hamani et al., 2005). In this study the midpoint of the STN at superior levels is found 9.9 mm lateral to the midline at superior levels and 9.7 mm lateral to the midline more inferiorly. This is comparable to other post mortem data (den Dunnen and Staal, 2005). Although it is important to note that our samples were not studied in a plane parallel to the AC-PC line, this variability again highlights the importance of direct visualisation of the STN for accurate localisation. Furthermore, increasing the MRI spatial resolution may improve the accuracy of STN localisation compared to current conventional approaches.

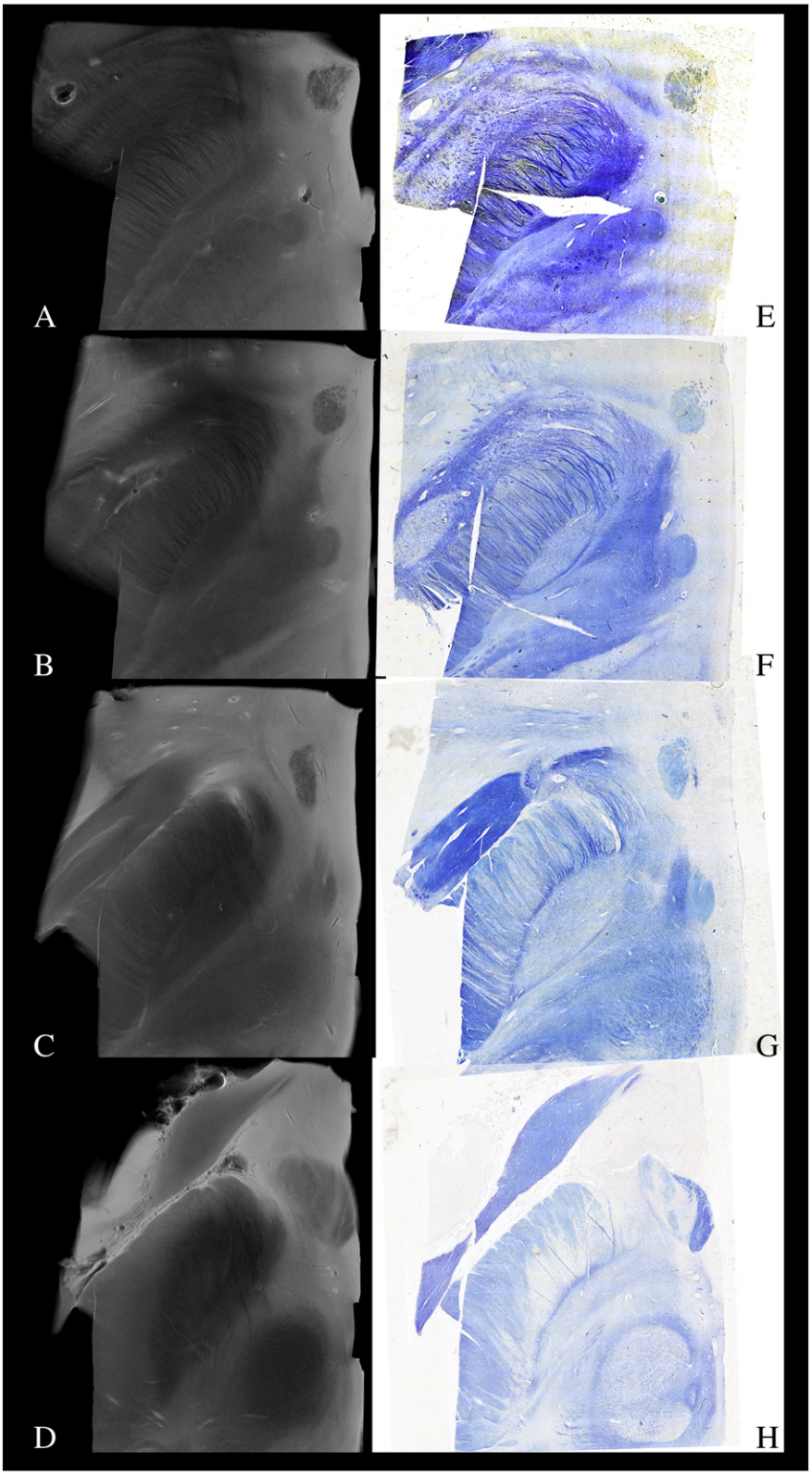

Fig. 6. Comparison of 9.4 T SE MRI images [A–D] and histological sections stained using the LFB/CV method [EG]. MRI in plane resolution 88 μm. Images are unlabelled to make comparison easier. For anatomical labels see Fig. 3. The STN is identified clearly as an almond shaped structure surrounded by white matter tracts (blue stain on LFB/CV images). LFB/CV staining within the STN was uniform in 4/4 cases with no particular anteromedial/posterolateral gradient evident. Structures corresponding to the borders of the STN can be clearly identified: at superior levels the LF can be seen as a dark blue myelinated structure corresponding to a region of hypointensity on T2w images [A and E]. One step inferiorly [B and F] the STN is clearly demarcated by a rim of dark blue staining and the fibres of the subthalamic fasciculus are seen radiating through the internal capsule—corresponding to the hypointensity seen on the anterolateral border of the STN on T2w/PDw images. The posteromedial border is clearly defined on the LFB/CV images as white matter tracts but on the MR images there is a relatively hyperintense signal arising from the region of the zona Incerta [B and F]. A region densely staining for myelin is seen separating the STN anteromedially from the superior SN posterolaterally on the LFB/CV image—this corresponds to a relatively hypointense region on the MR image [D and H]. It can be seen that the medial border of the STN is less clearly defined on the LFB/CV image at this level near the posterior aspect of the anteromedial tip on the LFB/CV image but this remains well defined on the 9.4 T SE MR image [H].

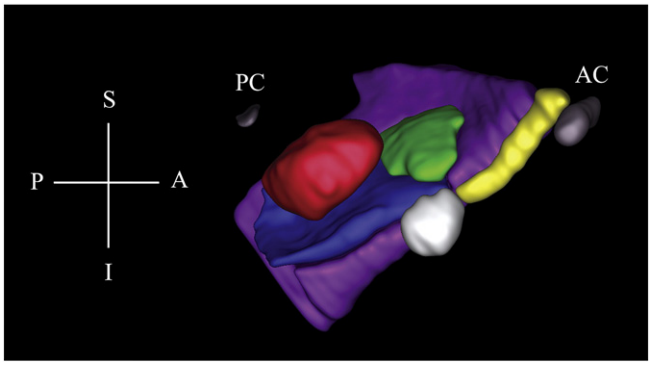

Fig. 7. Perl stain of the STN and environs. Serial axial sections through the subthalamic nucleus [A–F] from just above the STN [A] showing Prussian blue staining in the GP; in the STN Prussian blue staining is evident mostly in the medial half of the STN [B–D] and in the lower levels [D–F] intense staining of the SN pars reticulata is seen [D and E] just anterior to the STN.

Table 5
Distance in mm from the midpoint of the RN.

Distance from mid point of RN	Dorsal STN border	Ventral STN border	STN depth
Mean (Range)	4.3 (3.3–5.2)	7.5 (6.1–8.2)	3.6 (2.7–4.0)

Like others we found MR microscopy to be an excellent tool to display and study anatomy in three dimensions (Rijkers et al., 2007)—a feat which cannot be performed with standard histological techniques [Fig. 8]. This study lays the groundwork for future imaging of this region as high field MRI is becoming more widely available with clinical 3 T (Slavin et al., 2006) and 7 T machines enabling detailed study of the STN during life (Abosch et al., 2010; Cho et al., 2010). Furthermore, newer MR methodologies are improving our ability to accurately identify the STN during life (for review see (Massey and Yousry, 2010)) including added susceptibility (T2*) contrast using multiple gradient echoes (Elolf et al., 2007) susceptibility weighted imaging (Vertinsky et al., 2009) and fast grey matter acquisition T1 inversion recovery (Suhyadhom et al., 2009). However none of these methodologies have thus far been validated by comparison with histological material. The ability to image the STN during life at spatial resolutions similar to those reported *post mortem* herein would provide significant progress in both localisation accuracy for stereotactic surgery and the assessment of pathological changes in this nucleus.

Acknowledgments

We are indebted to the donors to the Queen Square Brain Bank for Neurological Disorders without whom this work would not have been possible. Part of this work has been presented and was awarded the Junior Award for Excellence in Clinical Research at the 12th International Congress of Parkinson's disease and Movement Disorders in Chicago in June 2008. LAM, HGP, MM and OA-H have all been supported by grants from the PSPA (Europe). MM has also been partially supported by AlBan, High Level Scholarship Programme of the European Union (2004–2006) and Caja de Seguro Social (CSS), Panama. OA-H has also been sponsored by the MBI Al Jaber Foundation. TY has also been supported by grants from the National Institute for

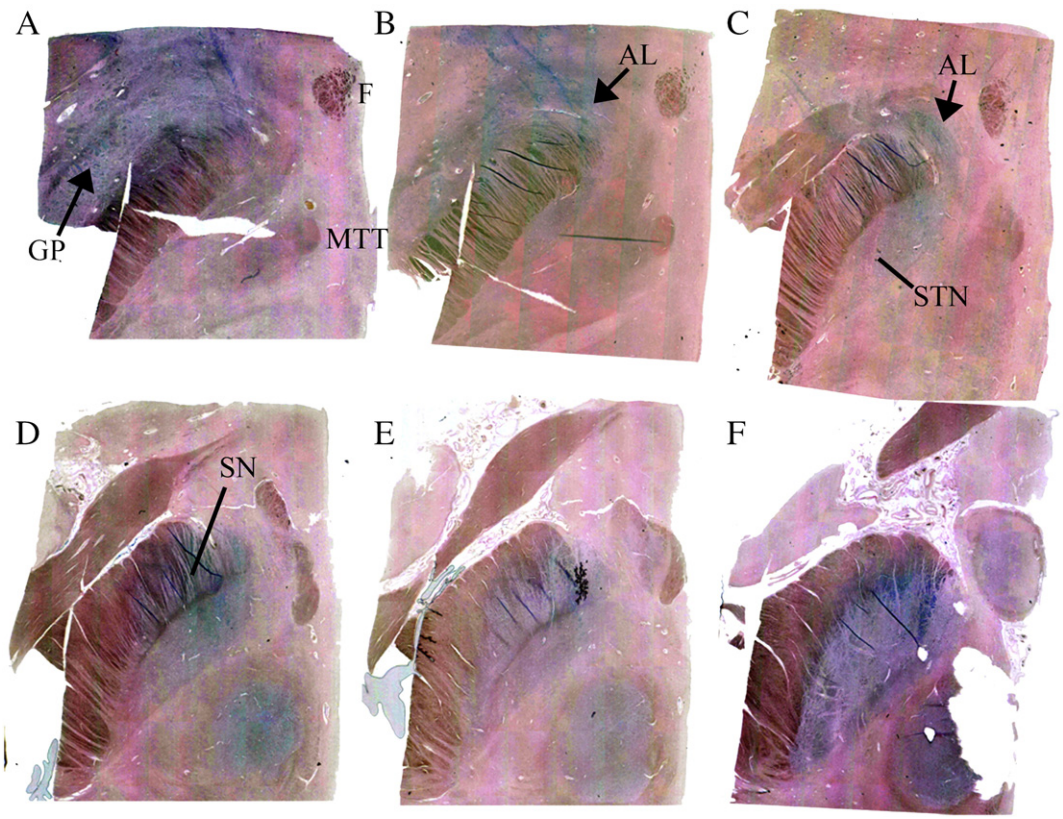

Fig. 8. Three-dimensional reconstruction viewed from the midline showing the relationship of the STN (green) to the internal capsule (purple), RN (red), SN (dark blue), MB (light grey), Fornix (yellow), AC and PC (dark grey, labelled) orientated so that the AC–PC line is horizontal. Orientation: S—superior, I—inferior, A—anterior, P—posterior.

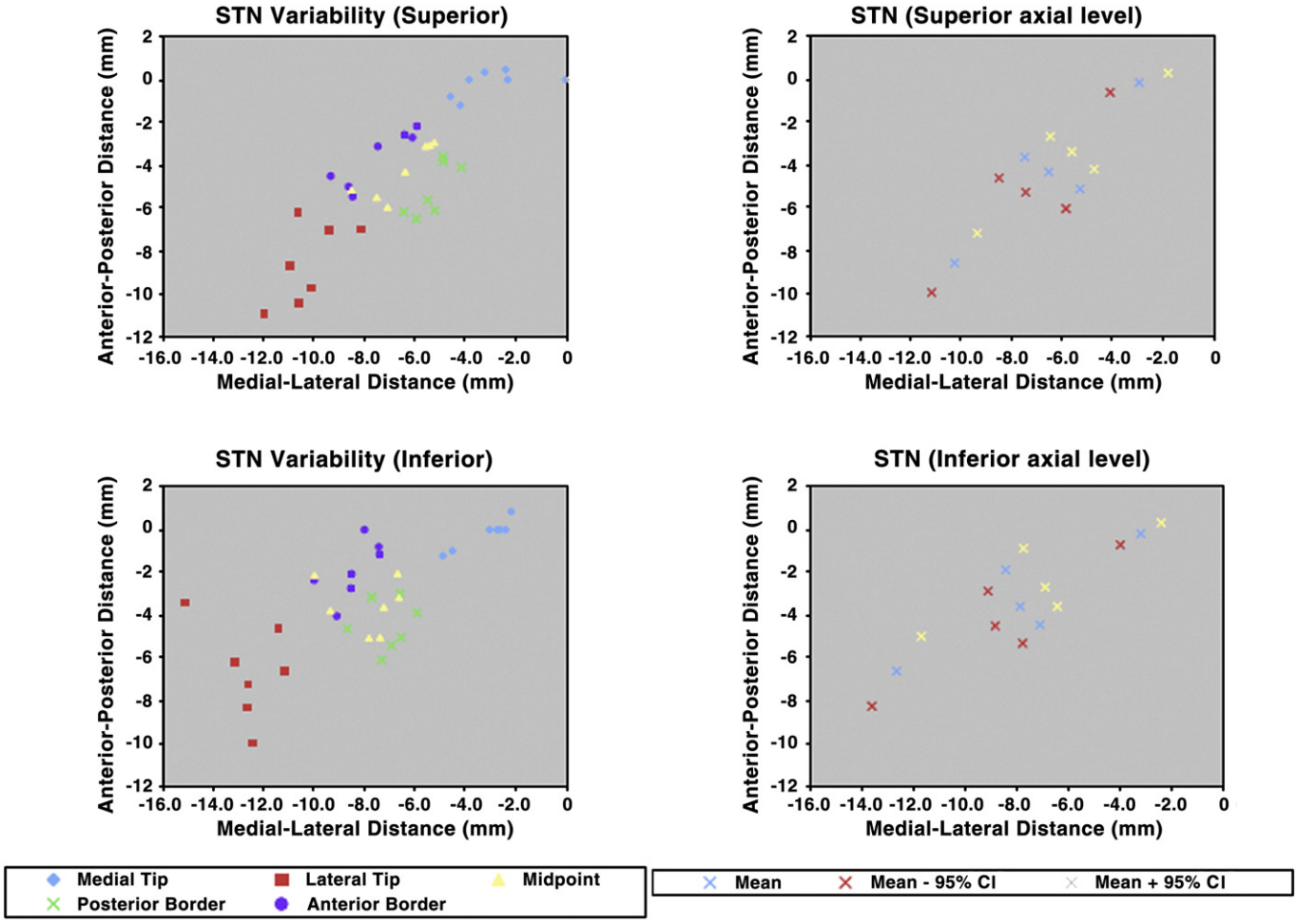

Fig. 9. Variability of the position of the STN. Scatter plots on the left include the measured locations of points for all available cases for superior and inferior levels examined. Scatter plots on the right show the mean position relative to the midpoint between the fornix and mamillothalamic tract in the axial plane. The upper and lower 95% confidence intervals are also plotted using coordinates in the *x*- and *y*-axis. Points plotted to give the profile of the STN are the medial and lateral tip, the anterior and posterior midpoints and the midpoint of the STN. See Fig. 11. All samples were reoriented such that the midpoint between the MTT and fornix is at position 0 in the *x*- and *y*-axis. See Table 3 for mean values and standard deviation.

Health Research, the Medical Research Council, the MS Society, the PSP Association (Europe), the British Heart Foundation, the Wellcome Trust, GSK, Biogen Indec and Novartis. The Unit of Functional Neurosurgery, Queen Square, London is supported by the Parkinson's Appeal. This work was undertaken at UCLH/UCL who received a proportion of funding from the UK Department of Health's National Institute for Health Research Biomedical Research Centres funding scheme (UCLH/UCL Comprehensive Biomedical Research Trust).

References

Abosch, A., Yacoub, E., Ugurbil, K., Harel, N., 2010. An assessment of current brain targets for deep brain stimulation surgery with susceptibility-weighted imaging at 7 tesla. Neurosurgery 67, 1745–1756 (discussion 1756).

Adachi, M., Hosoya, T., Haku, T., Yamaguchi, K., Kawanami, T., 1999. Evaluation of the substantia nigra in patients with Parkinsonian syndrome accomplished using multishot diffusion-weighted MR imaging. AJNR Am. J. Neuroradiol. 20, 1500–1506.

Ashkan, K., Blomstedt, P., Zrinzo, L., Tisch, S., Yousry, T., Limousin-Dowsey, P., Hariz, M.I., 2007. Variability of the subthalamic nucleus: the case for direct MRI guided targeting. Br. J. Neurosurg. 21, 197–200.

Aziz, T.Z., Peggs, D., Sambrook, M.A., Crossman, A.R., 1991. Lesion of the subthalamic nucleus for the alleviation of 1-methyl-4-phenyl-1,2,3,6-tetrahydropyridine (MPTP)-induced parkinsonism in the primate. Mov. Disord. 6, 288–292.

Bejjani, B.P., Dormont, D., Pidoux, B., Yelnik, J., Damier, P., Arnulf, I., Bonnet, A.M., Marsault, C., Agid, Y., Philippon, J., Cornu, P., 2000. Bilateral subthalamic stimulation for Parkinson's disease by using three-dimensional stereotactic magnetic resonance imaging and electrophysiological guidance. J. Neurosurg. 92, 615–625.

Benabid, A.L., Krack, P.P., Benazzouz, A., Limousin, P., Koudsie, A., Pollak, P., 2000. Deep brain stimulation of the subthalamic nucleus for Parkinson's disease: methodologic aspects and clinical criteria. Neurology 55, S40–S44.

Benazzouz, A., Gross, C., Feger, J., Boraud, T., Bioulac, B., 1993. Reversal of rigidity and improvement in motor performance by subthalamic high-frequency stimulation in MPTP-treated monkeys. Eur. J. Neurosci. 5, 382–389.

Bergman, H., Wichmann, T., DeLong, M.R., 1990. Reversal of experimental parkinsonism by lesions of the subthalamic nucleus. Science 249, 1436–1438.

Carpenter, M., Sutin, J., 1983. Human Neuroanatomy, 8th ed. Williams & Wilkins, Baltimore.

Cho, Z.H., Min, H.K., Oh, S.H., Han, J.Y., Park, C.W., Chi, J.G., Kim, Y.B., Paek, S.H., Lozano, A.M., Lee, K.H., 2010. Direct visualization of deep brain stimulation targets in Parkinson disease with the use of 7-tesla magnetic resonance imaging. J. Neurosurg. 113, 639–647.

Coenen, V.A., Prescher, A., Schmidt, T., Picozzi, P., Gielen, F.L., 2008. What is dorso-lateral in the subthalamic Nucleus (STN)?—a topographic and anatomical consideration on the ambiguous description of today's primary target for deep brain stimulation (DBS) surgery. Acta Neurochir. (Wien) 150, 1163–1165 (discussion 1165).

Counelis, G.J., Simuni, T., Forman, M.S., Jaggi, J.L., Trojanowski, J.Q., Baltuch, G.H., 2003. Bilateral subthalamic nucleus deep brain stimulation for advanced PD: correlation of intraoperative MER and postoperative MRI with neuropathological findings. Mov. Disord. 18, 1062–1065.

den Dunnen, W.F., Staal, M.J., 2005. Anatomical alterations of the subthalamic nucleus in relation to age: a postmortem study. Mov. Disord. 20, 893–898.

Dormont, D., Ricciardi, K.G., Tande, D., Parain, K., Menuel, C., Galanaud, D., Navarro, S., Cornu, P., Agid, Y., Yelnik, J., 2004. Is the subthalamic nucleus hypointense on T2-weighted images? A correlation study using MR imaging and stereotactic atlas data. AJNR Am. J. Neuroradiol. 25, 1516–1523.

Elolf, E., Bockermann, V., Gringel, T., Knauth, M., Dechent, P., Helms, G., 2007. Improved visibility of the subthalamic nucleus on high-resolution stereotactic MR imaging by added susceptibility (T2*) contrast using multiple gradient echoes. AJNR Am. J. Neuroradiol. 28, 1093–1094.

Foltynie, T., Zrinzo, L., Martinez-Torres, I., Tripoliti, E., Petersen, E., Holl, E., Aviles-Olmos, I., Jahanshahi, M., Hariz, M., Limousin, P., 2011. MRI-guided STN DBS in Parkinson's disease without microelectrode recording: efficacy and safety. J. Neurol. Neurosurg. Psychiatry 82 (4), 358–363.
Gross, R.E., Krack, P., Rodriguez-Oroz, M.C., Rezai, A.R., Benabid, A.L., 2006. Electrophysiological mapping for the implantation of deep brain stimulators for Parkinson's disease and tremor. Mov. Disord. 21 (Suppl. 14), S259–S283.
Hamani, C., Saint-Cyr, J.A., Fraser, J., Kaplitt, M., Lozano, A.M., 2004. The subthalamic nucleus in the context of movement disorders. Brain 127, 4–20.
Hamani, C., Richter, E.O., Andrade-Souza, Y., Hutchison, W., Saint-Cyr, J.A., Lozano, A.M., 2005. Correspondence of microelectrode mapping with magnetic resonance imaging for subthalamic nucleus procedures. Surg. Neurol. 63, 249–253 (discussion 253).
Hardman, C.D., Halliday, G.M., McRitchie, D.A., Morris, J.G., 1997. The subthalamic nucleus in Parkinson's disease and progressive supranuclear palsy. J. Neuropathol. Exp. Neurol. 56, 132–142.
Hardman, C.D., Henderson, J.M., Finkelstein, D.I., Horne, M.K., Paxinos, G., Halliday, G.M., 2002. Comparison of the basal ganglia in rats, marmosets, macaques, baboons, and humans: volume and neuronal number for the output, internal relay, and striatal modulating nuclei. J. Comp. Neurol. 445, 238–255.
Hariz, M.I., Krack, P., Melvill, R., Jorgensen, J.V., Hamel, W., Hirabayashi, H., Lenders, M., Wesslen, N., Tengvar, M., Yousry, T.A., 2003. A quick and universal method for stereotactic visualization of the subthalamic nucleus before and after implantation of deep brain stimulation electrodes. Stereotact. Funct. Neurosurg. 80, 96–101.
Hariz, M., Blomstedt, P., Limousin, P., 2004. The myth of microelectrode recording in ensuring a precise location of the DBS electrode within the sensorimotor part of the subthalamic nucleus. Mov. Disord. 19, 863–864.
Karachi, C., Yelnik, J., Tande, D., Tremblay, L., Hirsch, E.C., Francois, C., 2005. The pallidosubthalamic projection: an anatomical substrate for nonmotor functions of the subthalamic nucleus in primates. Mov. Disord. 20, 172–180.
Lane, J.I., Witte, R.J., Henson, O.W., Driscoll, C.L., Camp, J., Robb, R.A., 2005. Imaging microscopy of the middle and inner ear: Part II: MR microscopy. Clin. Anat. 18, 409–415.
Levesque, J.C., Parent, A., 2005. GABAergic interneurons in human subthalamic nucleus. Mov. Disord. 20, 574–584.
Limousin, P., Pollak, P., Benazzouz, A., Hoffmann, D., Broussolle, E., Perret, J.E., Benabid, A.L., 1995. Bilateral subthalamic nucleus stimulation for severe Parkinson's disease. Mov. Disord. 10, 672–674.
Limousin, P., Krack, P., Pollak, P., Benazzouz, A., Ardouin, C., Hoffmann, D., Benabid, A.L., 1998. Electrical stimulation of the subthalamic nucleus in advanced Parkinson's disease. N. Engl. J. Med. 339, 1105–1111.
Massey, L.A., Yousry, T.A., 2010. Anatomy of the substantia nigra and subthalamic nucleus on MR imaging. Neuroimaging Clin. N. Am. 20, 7–27.
McClelland 3rd, S., Vonsattel, J.P., Garcia, R.E., Amaya, M.D., Winfield, L.M., Pullman, S.L., Yu, Q., Fahn, S., Ford, B., Goodman, R.R., 2007. Relationship of clinical efficacy to postmortem-determined anatomic subthalamic stimulation in Parkinson syndrome. Clin. Neuropathol. 26, 267–275.
Moore, R.Y., Bhatnagar, R.K., Heller, A., 1971. Anatomical and chemical studies of a nigro-neostriatal projection in the cat. Brain Res. 30, 119–135.
Nieuwenhuys, R., Voogd, J., van Huijzen, C., 1988. The Human Central Nervous System: a synopsis and atlas, 3rd Revised ed.
Nieuwenhuys, R., Voogd, J., van Huijzen, C., 2008. The Human Central Nervous System: a synopsis and atlas, fourth ed.
Parent, A., 2002. Jules Bernard Luys and the subthalamic nucleus. Mov. Disord. 17, 181–185.
Parent, A., Hazrati, L.N., 1995. Functional anatomy of the basal ganglia. II. The place of subthalamic nucleus and external pallidum in basal ganglia circuitry. Brain Res. Brain Res. Rev. 20, 128–154.
Purdon Martin, J., 1927. Hemichorea resulting from a local lesion of the brain. (The syndrome of the body of Luys). Brain 50, 637–651.
Quester, R., Schroder, R., 1997. The shrinkage of the human brain stem during formalin fixation and embedding in paraffin. J. Neurosci. Methods 75, 81–89.
Rasbrand, W.S., 2009. Image J. U.S. National Institutes of Health, Bethseda, Maryland, USA. http://rsb.info.gov/ij/.
Rijkers, K., Temel, Y., Visser-Vandewalle, V., Vanormelingen, L., Vandersteen, M., Adriaensen, P., Gelan, J., Beuls, E.A., 2007. The microanatomical environment of the subthalamic nucleus. Technical note. J. Neurosurg. 107, 198–201.
Rutledge, J.N., Hilal, S.K., Silver, A.J., Defendini, R., Fahn, S., 1987. Study of movement disorders and brain iron by MR. AJR Am. J. Roentgenol. 149, 365–379.
Schaltenbrand, G., Wahren, W., 1977. Atlas for Stereotaxy of the Human Brain.
Silver, R.D., Djalilian, H.R., Levine, S.C., Rimell, F.L., 2002. High-resolution magnetic resonance imaging of human cochlea. Laryngoscope 112, 1737–1741.
Slavin, K.V., Thulborn, K.R., Wess, C., Nersesyan, H., 2006. Direct visualization of the human subthalamic nucleus with 3T MR imaging. AJNR Am. J. Neuroradiol. 27, 80–84.
Starr, P.A., 2002. Placement of deep brain stimulators into the subthalamic nucleus or Globus pallidus internus: technical approach. Stereotact. Funct. Neurosurg. 79, 118–145.
Suhyadhom, A., Haq, I.U., Foote, K.D., Okun, M.S., Bova, F.J., 2009. A high resolution and high contrast MRI for differentiation of subcortical structures for DBS targeting: The Fast Gray Matter Acquisition T1 Inversion Recovery (FGATIR). Neuroimage. doi:10.1016/j.neuroimage.2009.04.018.
Vertinsky, A.T., Coenen, V.A., Lang, D.J., Kolind, S., Honey, C.R., Li, D., Rauscher, A., 2009. Localization of the subthalamic nucleus: optimization with susceptibility-weighted phase MR Imaging. AJNR Am. J. Neuroradiol. 30 (9), 1717–1724.
Yelnik, J., 2002. Functional anatomy of the basal ganglia. Mov. Disord. 17 (Suppl. 3), S15–S21.
Yelnik, J., Bardinet, E., Dormont, D., Malandain, G., Ourselin, S., Tande, D., Karachi, C., Ayache, N., Cornu, P., Agid, Y., 2007. A three-dimensional, histological and deformable atlas of the human basal ganglia. I. Atlas construction based on immunohistochemical and MRI data. Neuroimage 34, 618–638.
Yushkevich, P.A., Piven, J., Hazlett, H.C., Smith, R.G., Ho, S., Gee, J.C., Gerig, G., 2006. User-guided 3D active contour segmentation of anatomical structures: significantly improved efficiency and reliability. Neuroimage 31, 1116–1128.
Zonenshayn, M., Rezai, A.R., Mogilner, A.Y., Beric, A., Sterio, D., Kelly, P.J., 2000. Comparison of anatomic and neurophysiological methods for subthalamic nucleus targeting. Neurosurgery 47, 282–292 (discussion 292–284).
Zrinzo, L., Zrinzo, L.V., Massey, L.A., Thornton, J., Parkes, H.G., White, M., Yousry, T.A., Strand, C., Revesz, T., Limousin, P., Hariz, M.I., Holton, J.L., 2011. Targeting of the pedunculopontine nucleus by an MRI-guided approach: a cadaver study. J. Neural Transm. 118 (10), 1487–1495.